Multielectron excitations at the L edges of barium in aqueous solution

P. D'Angelo, N. V. Pavel, and D. Roccatano
Dipartimento di Chimica, Università degli Studi di Roma ''La Sapienza,'' P.le Aldo Moro 5, 00185 Roma, Italy

H.-F. Nolting
European Molecular Biology Laboratory Outstation Hamburg, c/o Deutsches Elektronen-Synchrotron DESY, Notkestrasse 85, D-22603 Hamburg, Germany

(Received 20 May 1996)

An extensive investigation of the x-ray-absorption spectra above the L edges of a Ba^{2+} water solution is presented. Anomalous features are clearly detected in the spectra and have been associated with the creation of $2p4d$ and $2s4d$ double-core hole states for the L_3, L_2, and L_1 edges, respectively. A reliable determination of the double-electron edge parameters has been obtained by performing a combined L-edge analysis in the correct framework of the radial distribution function theory. Ba-O and Ba-H radial distribution functions have been calculated by means of molecular-dynamics simulations and have been used as relevant models in the calculation of the extended x-ray-absorption fine-structure (EXAFS) signals. The simultaneous analysis of the three edges allowed an unambiguous characterization of the multielectron transition affecting the L_1 cross section. The experimental values of the energy onsets of the double-electron features are in good agreement with previous theoretical calculations. The influence of multielectron transitions in the EXAFS data analysis is discussed. The neglect of double-electron excitation effects results in systematic errors on the structural parameters and in particular in an underestimation of the coordination numbers. [S0163-1829(96)02941-4]

I. INTRODUCTION

Recent research has revealed the presence of multielectron excitation effects in the x-ray-absorption spectra of several atomic and molecular systems.[1] The relative intensity of these effects is normally only a few percent of the single-electron transition and in condensed systems their identification is often hindered by the presence of the structured oscillating extended x-ray-absorption fine-structure (EXAFS) signal. Thus, most of the initial investigations on multielectron transitions were performed in the gaseous state.

Features associated with the creation of simultaneous K and M holes have been identified in the Ne,[2] Xe,[3] Ar,[4] and Kr (Ref. 5) absorption cross sections, being characterized either as a sudden jump, or as a slope change of the atomic background. The occurrence of double-electron excitations in condensed systems was first observed in Si K-edge spectra[6] and the existence of KL edge features was later found to be a characteristic of third-period atoms.[7] Strong KN and KM structures were identified above the Br,[8] Sr,[9] and Rb (Refs. 10 and 11) K edges in the absorption spectra of different systems.

Recently, several investigations of the EXAFS spectra of rare-earth-based materials have revealed the existence of resonances above the L edges.[12–14] These features were attributed to the excitation of $2s$ and $4d$ electrons in the case of the L_1 edge, and to the excitation of $2p$ and $4d$ electrons in the case of the L_2 and L_3 edges. A characterization of the energy onset of multielectron transitions was achieved by comparing the aqueous solution absorption spectra of the rare-earth series. The experimental values of the energy position of the double-excitation edges above the L_3 and L_2 edges, compared quite well with the theoretical values obtained from calculations based on many-body perturbation methods.[14,15] Less straightforward results have been obtained in the case of the L_1 edges, due to the poor signal-to-noise ratio of the experimental spectra. The presence of an anomalous feature associated with the $2p4d$ double-electron resonance was previously recognized in the L_3 absorption spectrum of a Ba^{2+} aqueous solution.[16] This study is limited to the L_3 edge and does not provide any quantitative characterization of the double-excitation channel.

The presence of multielectron transitions influences the EXAFS structural analysis by introducing unexpected peaks at low distance values in the Fourier transform (FT) of the spectrum and modifying its intensity. As a consequence, the structural parameters obtained from the data analysis are affected by systematic errors, and this effect is more important for coordination numbers.[9] In disordered systems, where multielectron background features may be of comparable intensity to the weak structural oscillations, the standard background subtraction is totally inadequate. Therefore, it is crucial to develop a data analysis method which allows multielectron transitions to be detected and properly accounted for. A new improved method, which uses a background empirical model to properly account for double-electron excitations, has been successfully employed in the analysis of different systems.[8,9] Several other methods have appeared in the literature.[17]

The aim of the present paper is to provide a deeper insight into multielectron transition processes affecting the Ba L edges. For this purpose we chose a Ba^{2+} aqueous solution where the EXAFS oscillations are expected to be weak, due to the large structural disorder.

A method which uses molecular-dynamics (MD) radial distribution functions as relevant models in the calculation of the EXAFS structural signal has been employed to study the hydration shells of Br^-,[18] Rb^+,[11] and Sr^{2+}.[9] This method

provides a reliable determination of the structural signal associated with the water molecules. Removal of the EXAFS oscillations from the absorption spectrum allows the isolation of the multielectron transition features and the identification of their position. L_3 absorption spectra of Ba^{2+} aqueous solutions were previously studied[19] and the EXAFS analysis was performed without including multielectron excitation effects in the atomic background. The narrow available energy range of the spectrum hampered a conclusive determination of the structural parameters. In the present work, a combined L-edge data analysis has been carried out. Very accurate structural results have been obtained by performing a multiple-edge refinement, even though the available energy range for each edge is quite limited. This approach was previously employed in the study of the short-range structure of liquid and crystalline Sn.[20] The presence of multielectron transitions involving $2p4d$ electrons has been detected for the Ba L_3 and L_2 edges. The simultaneous analysis of the three edges allowed an unambiguous identification of multielectron excitation affecting the L_1 edge. A careful analysis has been performed in order to quantify the effect of neglecting double-electron excitation effects on the structural parameters. The results of the present investigation represent a valid tool in the study of absorption spectra above the L edges of other systems.

The paper is organized as follows. In Sec. II the results of the MD computational procedure for the Ba^{2+} aqueous solution are presented. The experimental details are given in Sec. III. In Sec. IV the evidence for the double-excitation channels in the raw data is discussed. In Sec. V the multiedge data analysis method is described and the results are given in Sec. VI.

II. MOLECULAR-DYNAMICS COMPUTATIONAL PROCEDURE

Molecular-dynamics (MD) simulations were performed using an isothermal-isobaric simulation algorithm.[21] The temperature was kept constant at 300 K by weak coupling to an external temperature bath with a coupling constant of 0.1 ps. The pressure was also kept constant by coupling to a bath with a coupling constant of 0.5 ps. Simulations were carried out using a rectangular box consisting of one Ba^{2+} ion and 197 water molecules subjected to periodic boundary conditions. All the MD runs were performed using the program package GROMOS87.[22] The applied empirical force field contains terms representing bond angle bending, van der Waals, and electrostatic interactions.[22] The Lennard-Jones parameters used in the present study for Ba^{2+} were reported by Åqvist.[23] The simple point-charge model was used for water.[24] The SHAKE algorithm was used to constrain bond lengths.[25] A dielectric permittivity, $\varepsilon=1$, and a time step of 2 fs were used. The cutoff radius for the nonbonded interactions was 8 Å. All atoms were given an initial velocity obtained from a Maxwellian distribution at the desired initial temperature. After the initial minimization of the system, the MD simulations were performed. The first 40 ps were used for equilibration and the following 100 ps were used for the analysis. The trajectories were saved every 25 time steps.

The Ba-O and Ba-H radial distribution functions $g(r)$ and the corresponding running integration numbers are reported in Fig. 1. The $g_{\mathrm{Ba,O}}(r)$ shows a very sharp first peak centered at 2.8 Å. The integration over this first peak gives a coordination number N_{O} of about 9. This value is 0.8 lower than the one obtained by Spohr *et al.*[26] for Sr^{2+} in water. This finding is justified by the difference of the interaction potentials used in the simulations. The zero values assumed by the $g_{\mathrm{Ba,O}}(r)$ between the first and second peak indicate the presence of a well-defined hydration shell around the cation. The nearest-neighbor peak in the $g_{\mathrm{Ba,H}}(r)$ is situated at 3.4 Å and the running integration number is about 18, which is in agreement with the N_{O} value. Figure 2 shows the solvent-solvent pair-distribution functions compared with the ones obtained for the solvent alone. The most interesting features are the small decrease of the height of the first peak in the $g_{\mathrm{O,O}}(r)$ with respect to pure water, and the less shallow first minimum, as a consequence of a slightly higher asymmetry of the first peak. In the $g_{\mathrm{O,H}}(r)$ and $g_{\mathrm{H,H}}(r)$ we note also a

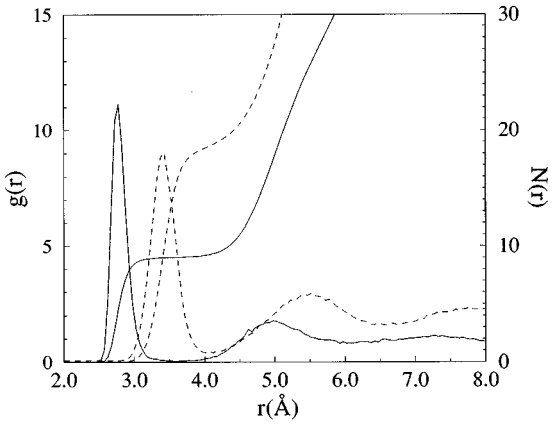

FIG. 1. Ba-O (solid line) and Ba-H (dashed line) pair-distribution functions as derived from MD simulations for Ba^{2+} in water (left scale) and corresponding integration numbers (right scale).

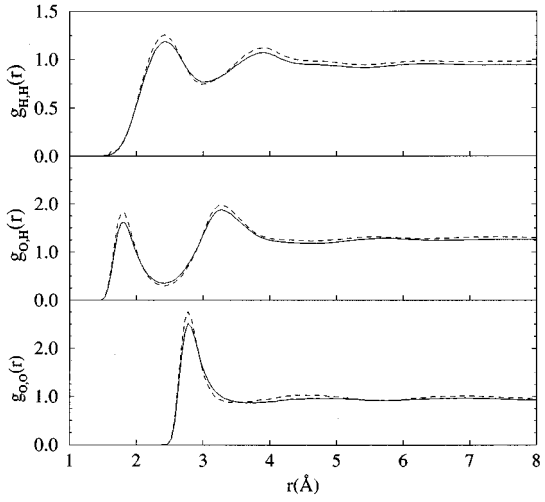

FIG. 2. O-O, O-H, and H-H pair-distribution functions as derived from MD simulations for Ba^{2+} in water (solid line) compared with the same obtain from MD simulations of pure water (dashed line).

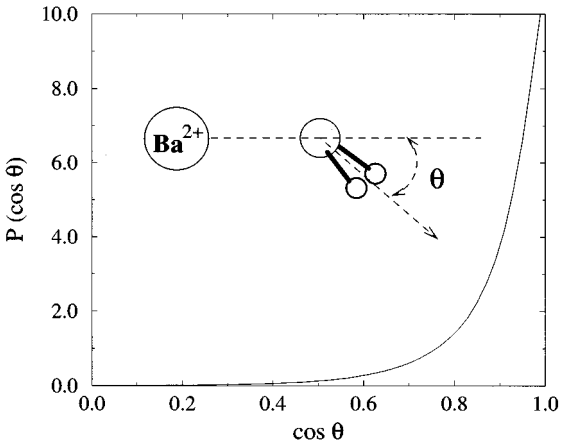

FIG. 3. Distribution of $\cos\theta$ for the water molecules in the first hydration shell of Ba^{2+}.

decrease of the first peak and the shallowing of the minimum with respect to pure water.

The orientation of the water molecules with respect to the ion is described by the cosine of the θ angle between the dipole moment vector pointing from the oxygen to the ion (see inset in Fig. 3). The resulting distribution (see Fig. 3) shows a dominant peak centered at $\cos\theta=1$ and an average value at $\cos\theta=0.6$ corresponding to $\theta=53°$. These values account for the weaker structuring ability of Ba^{2+} with respect to other alkaline-earth ions,[27] as expected due to its large ionic radius.

The geometric properties of the hydration shell of Ba^{2+} was studied in detail using a method proposed by Pálinkás *et al.*[28] for the study of the Mg^{2+} hydration geometry. The positions of the hydration water molecules are defined using an appropriate local coordinate system. In this system the ion defines the origin, the oxygen atom of a first water molecule of the hydration shell defines the z positive axis and the oxygen of a second water molecule the xz plane. The arbitrary fixing of one of these molecules to define such a coordinate system introduces some distortions in the statistics. In order to reduce some of these effects, each water molecule in the hydration shell was used to define the positive z axis. The recording of the oxygen atomic positions in the ion-center coordinate system over the whole simulation run provides the three-dimensional water distribution in the hydration shell. The projections of the distribution onto the three planes of this coordinate system are shown in Fig. 4 in the form of density maps. These density maps show the existence of a high degree of order of the hydration shell water molecules, but it is not possible to find a regular symmetry in the pictures. Another way to quantitatively observe this high degree of order is the use of the angular distribution function of the oxygen-ion-oxygen angles (see inset in Fig. 5). $P(\cos\phi)$ as function of $\cos\phi$ is shown in Fig. 5. The maxima in $P(\cos\phi)$ indicate two favorable angles at 140° and 70°. The shape and the position of the spots in the density maps resemble those obtained by Probst *et al.* for Ca^{2+} (Ref. 29) (for this ion a coordination number of about 9 was found) and the $\cos\phi$ distribution is similar to the one obtained by Kowall *et al.*[30] for the nine-coordinate Nd^{3+} and Sm^{3+} ions. In this work the possible polyhedral structures of water molecules in the hydration shell are discussed in detail.

III. EXPERIMENTAL SECTION

The aqueous solution was prepared by solubilizing $BaCl_2$ in deionized water at a concentration of 0.1 M. The absorption spectra at the L edges were recorded in transmission mode using the EMBL spectrometer at HASYLAB.[31] Measurements were performed at room temperature with a Si(111) double-crystal monochromator[32] and 50% of harmonic reject achieved by slightly detuning the two crystals from parallel alignment. Five spectra for each edge were recorded and averaged after performing an absolute energy calibration.[33] The DORIS II storage ring was running at an energy of 4.45 GeV with electron currents between 70 and 40 mA. The solution was kept in a cell with a 0.8 mm Teflon spacer and Kapton film windows. From the width of the peaks of the calibrator[33] the energy resolution of the Si(111) monochromator could be determined experimentally as 0.7 eV at 5112 eV.

IV. OBSERVED SPECTRA

In the standard EXAFS analysis the structural oscillation is extracted from the raw absorption spectrum subtracting a background function modeled as a smooth polynomial spline. Multielectron excitations are usually associated with the presence of slope changes and unexpected features in the atomic background. These have to be accounted for to perform a reliable structural analysis. Aqueous solutions of ions at room temperature are ideal samples to highlight multiexcitation effects. Due to the small amplitude of the oxygen and hydrogen atoms and to structural disorder, the EXAFS contribution to the absorption cross section is weak and is confined to the low-energy region of the spectrum and double-electron excitation features are clearly visible in the raw spectra.

The absorption cross sections at the Ba L_3, L_2, and L_1 edge are shown in Fig. 6. The spectra are normalized to the absorption discontinuity at each edge and are offset vertically by 0.7 units, for clarity. The zero of the energy scale refers to each respective threshold, defined by the first inflection point of the absorption spectra. A careful inspection of the magnified region of the spectra shown in the inset, reveals the presence of anomalous features around 110 eV which are similar to the double-excitation structures observed in the absorption spectra of some rare-earth ions in aqueous solutions.[12–14] These features were attributed to the simultaneous excitation of $2s$ and $4d$ electrons in the case of the L_1 edge and to the excitation of $2p$ and $4d$ electrons in the case of the L_2 and L_3 edges. An unambiguous characterization of these multielectron transitions has been obtained from the experimental data with use of a proper background model as described in Sec. V. The modules of the Fourier transform (FT) of the L_3, L_2, and L_1 EXAFS spectra extracted with a three segmented cubic spline, performed in the interval 2.8–9.5 $Å^{-1}$ (2.7–8.5 $Å^{-1}$ in the case of the L_1 edge) are shown in Fig. 7. Beside the structural peak at about 2.3 Å, corresponding to the first coordination shell, a further peak is observed at about 1.0 Å, which cannot be assigned to any structural origin. The presence of these unexpected low-

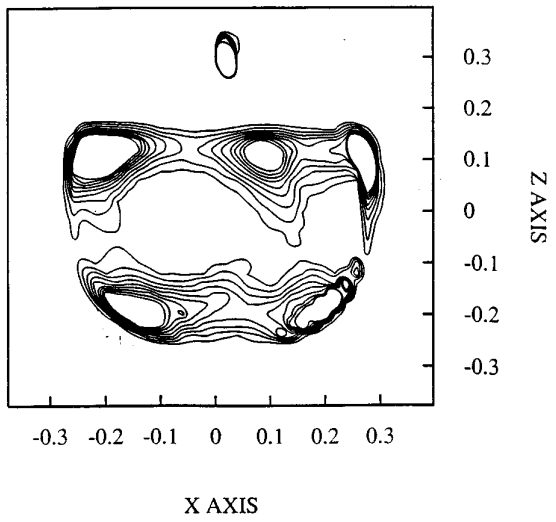

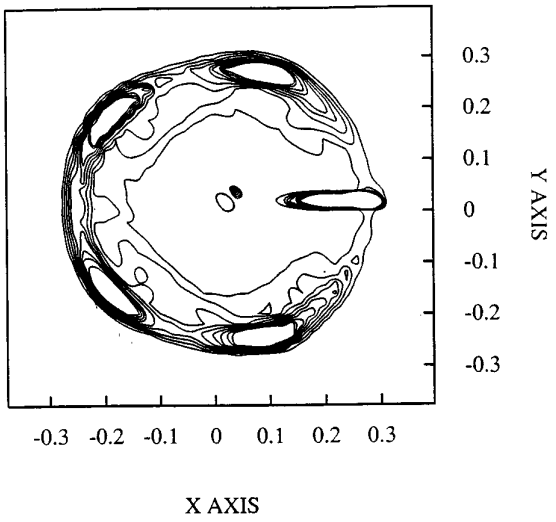

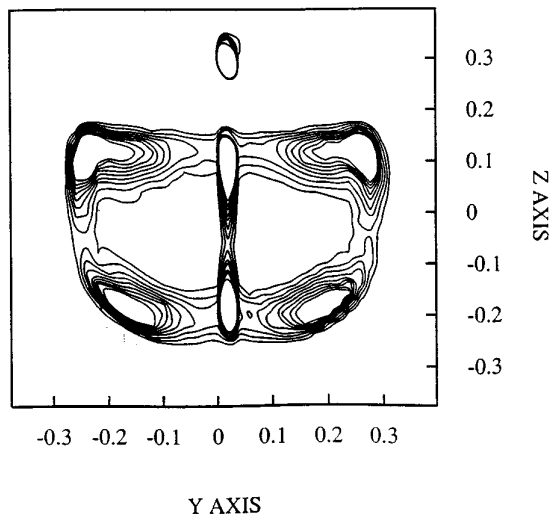

FIG. 4. Density maps of the projections of the oxygen atom positions of the nine nearest-neighbor water molecules around Ba^{2+} onto the planes of an ion-centered coordinate system, as defined in the text, calculated from MD simulations. The normalized isolines are evaluated from 0.006 to 0.030 using an incremental step of 0.003.

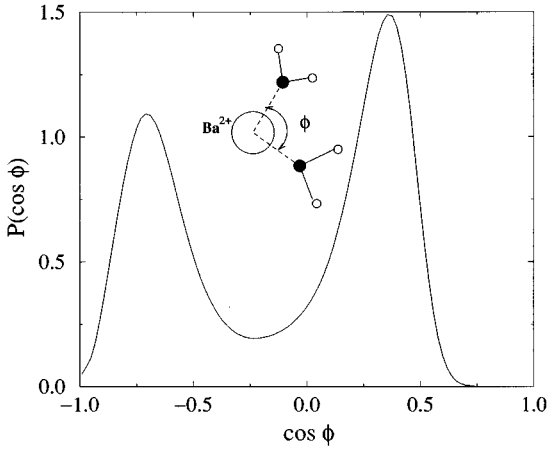

FIG. 5. Probability distribution for the angle ϕ formed by the ion and all pairs of water oxygens that belong to the first hydration shell.

distance peaks is indirect evidence of the presence of multielectron excitations in the atomic background, as already observed for several other systems.[8,9]

V. METHOD FOR DATA ANALYSIS

In the present work a multiedge analysis has been carried out. The model signal associated with a set of M different atomic edges is given by the relation:

$$\alpha_{\mathrm{mod}}(E)=\sum_{i=1}^{M}\left[j_i\sigma_0^{(i)}(E)(1+S_0^{2(i)}\chi^{(i)}(E-E_0^{(i)}))\right]+\beta(E), \tag{1}$$

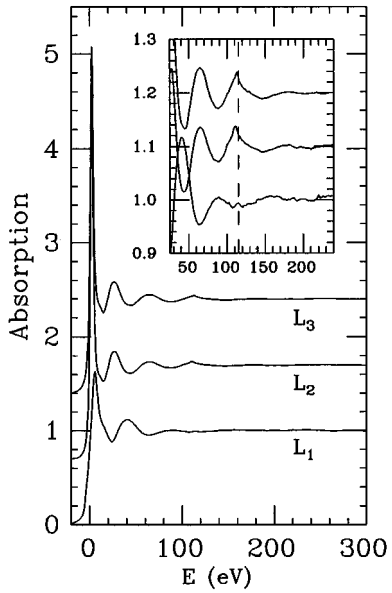

FIG. 6. Normalized absorption spectra of Ba^{2+} in water near the L edges. The spectra show the presence of anomalous features (indicated by dashed lines in the inset) due to the $2p4d$ and $2s4d$ double-electron transitions. The zero of the energy scale refers to each respective threshold defined by the first inflection point of the absorption spectrum. The spectra are offset vertically by 0.7 units.

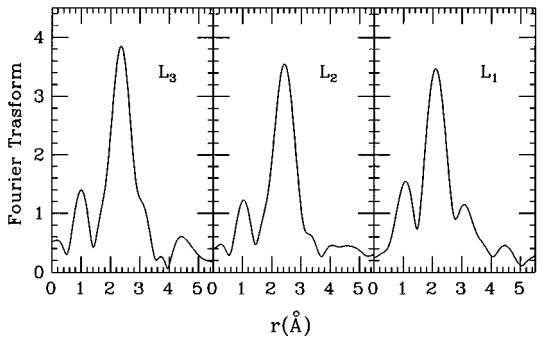

FIG. 7. Magnitude of the Fourier transform of the Ba^{2+} aqueous solution L_3, L_2, and L_1 spectra. The peaks around 1.0 Å have no structural meaning and are due to the double-electron excitation effects.

where $\sigma_0^{(i)}$ is the atomic cross section of the ith considered absorption channel, j_i is a scaling factor accounting for the actual density of the photoabsorber atoms, $\chi^{(i)}$ is the EXAFS signal containing the structural information related to the ith edge, $S_0^{2(i)}$ provides a uniform reduction of the signal and is associated with many-body corrections to the one-electron cross section, $E_0^{(i)}$ defines the relation between the theoretical and the experimental energy scales, and $\beta(E)$ is the background function, which accounts for further absorbing processes. Multielectron excitation channels are accounted for by modeling the $\beta(E)$ function as the sum of a smooth polynomial spline plus step-shaped functions. Each function depends on three parameters: the double-electron edge position relative to the single-hole state ΔE, its width ΔD, and the relative jump H.[8] Fits of the $\alpha_{\mathrm{mod}}(E)$ to the raw data allow the determination of these parameters and the experimental characterization of the multielectron transitions channels.

The structural and background parameters are optimized by performing a comparison between the $\alpha_{\mathrm{mod}}(E)$ theoretical signal and the experimental spectrum. The model signal $\alpha_{\mathrm{mod}}(E)$ is refined by minimizing a square residual function of the type:

$$R(\{\lambda\})=\sum_{i=1}^{\mathcal{N}} \frac{[\alpha_{\mathrm{exp}}(E)-\alpha_{\mathrm{mod}}(E_i;\lambda_1,\lambda_2,\ldots,\lambda_p)]^2}{\sigma_i^2}, \quad (2)$$

where $\mathcal{N}$ is the number of experimental points E_i, $\{\lambda\}=(\lambda_1,\lambda_2,\cdots,\lambda_p)$ are the p parameters to be refined, and σ_i^2 is the variance associated with each experimental point $\alpha_{\mathrm{exp}}(E)$.

Use of a multiedge analysis gives rise to several advantages. Firstly, the number of experimental points which are used to derive the structural information is strongly increased. Secondly, a reliable determination of the refined parameters can be achieved even when only a narrow energy range is available and the EXAFS spectra of different absorption channels are overlapped. Finally, for multielement systems partial contributions to the total structural signal are better defined.

In the standard EXAFS analysis a set of Gaussian shells is usually employed to describe the coordination of the photoabsorber atom. This method can produce significant errors in the determination of the structural parameters for systems which present anharmonic thermal vibrations or interatomic asymmetric pair-distribution functions. Frequently, for disordered systems, the neglect of asymmetry leads to unreliable results even when an apparently reasonable fit to the experimental data is obtained.[34,35] When the EXAFS technique is used to determine the structure of disordered materials, $\chi(k)$ must be represented by the general equation[36]

$$\chi(k)=\sum_j \int_0^\infty g_j(r)4\pi r^2\rho_j A_j(k,r)\sin[2kr+\phi_j(k,r)]dr, \quad (3)$$

where $g_j(r)$ is the radial distribution function associated with the jth species, $A_j(k,r)$ and $\phi_j(k,r)$ are the amplitude and phase functions, respectively, and ρ_j is the density of the scattering atoms. The high-distance contribution of the $\chi(k)$ signal is damped by the photoelectron mean free path $\lambda(k)$ through an exponential function of the type $\exp[-r/\lambda(k)]$ which leads to an effective upper integration limit of 5–8 Å in Eq. (3). In our calculation the mean free path $\lambda(k)$, as well as the additional damping factor accounting for the monochromator resolution, is included in the amplitude function $A_j(k,r)$.

Recently, it has been shown that the EXAFS data analysis of disordered systems can benefit strongly from the use of pair-distribution function models obtained from diffraction data or computer simulations in the calculation of the structural signal.[9,11,18,37] In the present investigation the $\chi(k)$ theoretical signals associated with water molecules have been calculated starting from the Ba-O and Ba-H pair-distribution functions obtained from the MD simulations. Due to the low resolution (0.05 Å), the shape of the first rise of the calculated $g(r)$'s may not be accurate. The high short-range sensitivity of the EXAFS technique can be used to improve the low-distance region of the MD $g(r)$'s by refining the peak parameters on the basis of the x-ray-absorption data. Initial asymmetric peaks are obtained decomposing the MD $g(r)$'s into an asymmetric peak and a long-distance tail. The tail contribution is usually calculated using Eq. (3) and is kept fixed in the refinement. In our case the Ba-O and Ba-H tail signals have been found to be negligible and therefore they have not been considered. As previously described,[18] the asymmetric peaks are modeled with a Γ-like distribution function which depends on four parameters, namely the coordination number N, the average distance R, the mean-square variation σ^2 and the skewness β. These parameters are optimized by fitting the EXAFS theoretical signal to the experimental data allowing the refinement of the short-range shape of the MD $g(r)$'s.

Ab initio calculations of the L_3, L_2, and L_1 x-ray-absorption cross section and the configurational averages have been performed using the GNXAS program set.[38] Phase shifts and amplitudes have been calculated starting from one of the MD configurations by using muffin-tin potential and advanced models for the energy-dependent exchange-correlation self-energy (Hedin-Lundqvist).[39] The muffin tin radii used where 1.90, 0.90, and 0.22 Å for barium, oxygen, and hydrogen atoms, respectively. Inelastic losses of the photoelectron in the final state are accounted for intrinsically by complex potentials. The imaginary part also includes a constant factor accounting for the core-hole widths. The only nonstructural parameters which have been minimized are

TABLE I. $L_{2,3}N_{4,5}$ and $L_1N_{4,5}$ transition intensities and excitation energies. The absorption discontinuities H are given in the corresponding L-edge jump units. The excitation energies ΔE are relative to the corresponding single-hole state. All the energies are given in eV. Theoretical data have been taken from Refs. 14 and 15. σ_D and σ_S represent the cross-section strength for the double- and single-electron absorption processes, respectively.

Edge	H %	ΔE (exp)	ΔE (theo)	$Z+1$	σ_D/σ_S (exp) %	σ_D/σ_S (theo) %
$L_3N_{4,5}$	4.1	114	110	102–105	0.8	2.54
$L_2N_{4,5}$	3.9	112	110	102–105	0.9	2.54
$L_1N_{4,5}$	2.8	120	111	102–105	0.6	2.45

$E_0^{(i)}$ and $S_0^{2(i)}$, while a fixed value of the monochromator resolution was used during the minimization of each absorption edge.

VI. RESULTS AND DISCUSSION

In this section the combined L-edge data analysis of the Ba^{2+} aqueous solution is described. The main contribution to the EXAFS structural signal is related to the first-neighbor peak of the Ba-O and Ba-H radial distribution functions. The Ba-O and Ba-H first-shell peaks are described by Γ-like functions with $R_O=2.80$ Å, $\sigma^2{}_O=0.012$ Å^2, $\beta_O=0.62$, $N_O=8.7$, and $R_H=3.46$ Å, $\sigma^2{}_H=0.036$ Å^2, $\beta_H=0.60$, $N_H=18.4$, respectively. These parameters have been derived using a least-square fitting on the MD $g(r)$'s. The $\chi(k)$ signals associated with the Ba-O and Ba-H asymmetric peaks have been calculated for the three L edges using the GNXAS program[38] and a fitting procedure has been applied to the peak parameters in order to obtain the best fit between the theoretical and the experimental signals. This approach provides a reliable estimate of the structural contribution to the absorption cross section allowing the background parameters to be fitted and correctly determined. Least-squares fits of the three L-edge experimental cross sections have been performed simultaneously using the FITHEO program[38] and a weighting value of 2.0 has been applied. For each absorption cross section a step-shaped function has been included in the atomic background to account for the $2p(2s)4d$ double-excitation edges. In Table I the double-electron edge experimental parameters obtained from the fitting procedure are listed: ΔE is the energy of the double-excitation channels relative to the single-hole state and the intensity H is measured in the corresponding L-edge jump units. The energy location of these features roughly corresponds to the predictions of the $Z+1$ approximation. Applying this approximation means that we consider the $2p$ (or $2s$) hole to be completely screened prior to the second excitation taking place. However, this is a crude approximation as indicated by the disagreement between the experimental and the predicted values. In order to unambiguously assign the structures observed to a specific many-body transition, we have compared our results with the theoretical values obtained by Chaboy and co-workers[15] from many-body perturbation methods. According to these *ab initio* calculations the main double-excitation channels affecting the $L_{2,3}$ and L_1 edges correspond to the $2p4d\rightarrow(5d)^2$ and to the $2s4d\rightarrow6p5d$ transitions, respectively (namely $L_{2,3}N_{4,5}$ and $L_1N_{4,5}$). The experimental energy onset of the $L_{2,3}N_{4,5}$ and $L_1N_{4,5}$ edges is in good agreement with the theoretical predictions, as listed in Table I.

In Fig. 8 the best-fit analysis for the Ba L_3, L_2, and L_1 EXAFS spectra (left, middle, and right panels, respectively) are presented. The first two curves from the top of each panel represent the Ba-O and Ba-H structural signals. The remainder of the figure shows the total theoretical contributions compared with the experimental spectra and the resulting residuals. In Fig. 8 the dashed curves are the continuation of the EXAFS signal associated with the previous edge. In the present case these contributions are negligible, but for systems with more structured signals the distortion of the $\chi(k)$ curve due to the overlap of different absorption edges can be important. The overall agreement between the experimental and theoretical signals is excellent and a $R=0.599\times10^{-8}$ has been obtained. The agreement is slightly worse for the L_1 edge, due to the larger noise of the spectrum. However, also in this case the residual curve contains experimental noise, only. Note that the structural signals are dominated by the Ba-O signals, while the Ba-H contributions are weaker and mainly affect the low-k region of the spectra. Nevertheless, as previously observed,[9,37] the inclusion of the hydrogen signals has been found to be essential to properly reproduce the experimental spectra in the low-k region.

As already observed in other cases,[9,11] the step-shaped

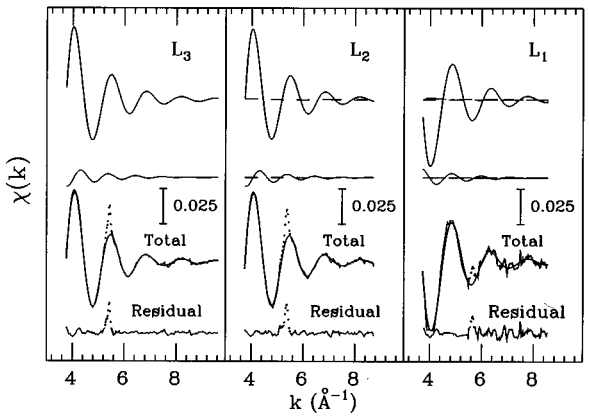

FIG. 8. Fit of the Ba^{2+} aqueous solution L_3, L_2, and L_1 spectra (left, middle, and right panel, respectively). From top to bottom of each panel the following curves are reported: Ba-O and Ba-H theoretical signals, sum of the previous contributions compared with the experimental spectrum and residuals. The dashed curves are the extensions of the EXAFS signals related to the previous edges. The dots are the experimental points excluded from the fitting procedure.

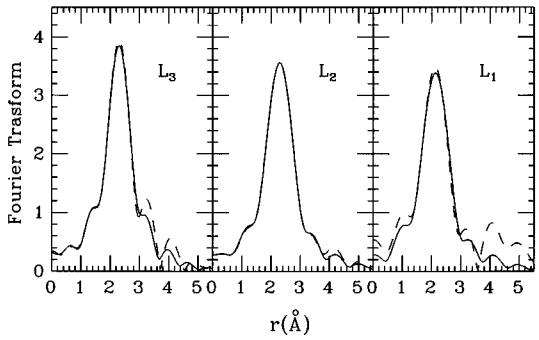

FIG. 9. Fourier transforms of the Ba^{2+} aqueous solution L_3, L_2, and L_1 experimental spectra (dashed line) compared with the total theoretical signals (solid line). The $\chi(k)$ experimental signals have been obtained by subtracting an atomic background which includes the double-electron excitation edges.

function used in the extraction of the structural signal, accounts only for the slope change and the discontinuity associated with the opening of the double-excitation channels. Additional features above the multielectron excitation edges will still remain in the structural signal as nonstructural peaks. A sharp feature is clearly visible in the Ba L_3, L_2, and L_1 EXAFS spectra and residuals at about 5.4 $Å^{-1}$. In order to perform a reliable determination of the structural parameters, the experimental points in a range of approximately 20 eV around these peaks have been excluded from the fitting procedure. It is not surprising that the L_3 and L_2 EXAFS spectra are very similar, while the L_1 one is different, due to the different symmetry of the channels. In the latter case the double-electron resonance feature is located at the oscillation minimum and its intensity is weaker as compared with that affecting the L_3 and L_2 EXAFS spectra. The same trend has been found by Chaboy and co-workers[15] from *ab initio* calculations.

Figure 9 shows the comparison of the Fourier transforms of the calculated and experimental spectra in the range 3.8–9.6, 3.7–8.7, and 3.7–8.6 $Å^{-1}$ for the L_3, L_2, and L_1 edge, respectively, obtained after removal of the double-excitation channels. The low-distance peaks are no longer present and a very good agreement between the theoretical and experimental curves has been obtained. The high-frequency peaks in the FT of the L_1 experimental signal are due to the noise of the spectrum.

For the structural analysis it is important to assess the intensity of the double-excitation effects with respect to the EXAFS amplitude. For this purpose Chaboy and co-workers[15] computed the ratio between the double- and single-electron line strength. An experimental estimate of the intensity of the main $2p \rightarrow 5d$ and $2s \rightarrow 6p$ bound transitions has been obtained by applying a deconvolution model to the L_3, L_2, and L_1 cross sections. The threshold region of the spectra has been deconvoluted as a sum of an arctangent function describing the transition into the continuum, and a Lorentzian function representing the transition from the $2p(2s)$ to the $5d(6p)$ state. The two functions have been convoluted with a Gaussian function accounting for the experimental resolution. The deconvolution process has been performed using a least-square fitting procedure on the threshold region of the normalized spectra. The results of

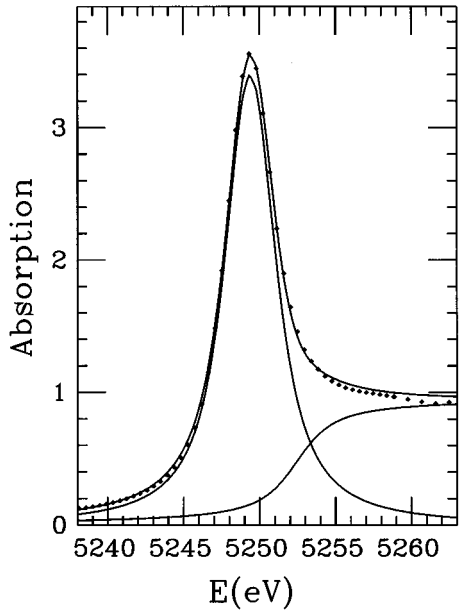

FIG. 10. Deconvolution of the L_3-edge normalized absorption spectrum of the Ba^{2+} aqueous solution (dots) as sum of an arctangent function, describing the transition into the continuum, and a Lorentzian function, representing the transition to the $5d$ bound state.

this procedure are shown in Fig. 10 for the L_3 edge. The energy positions of the single-hole transitions were found at 5249, 5626, and 5999 eV, for the L_3, L_2, and L_1 cross section, respectively. From the minimization the transition into the continuum states has been found to occur 2 eV above the $2p(2s) \rightarrow 5d(6p)$ transition, for the three edges. The resolution values obtained from the fitting procedure are 0.7, 0.9, and 2.1 eV for the L_3, L_2, and L_1 edges, respectively. These results are in excellent agreement with the value determined from the calibrator; as expected the experimental resolution value increases with energy. The core-hole width Γ (half width at half maximum) which optimized the agreement between the model and the experiment resulted $\Gamma(L_3)=1.66$, $\Gamma(L_2)=1.78$, and $\Gamma(L_1)=2.00$ eV, which compare well with semiempirical evaluations.[40] These values have been directly included in the calculation of the Ba-O and Ba-H EXAFS theoretical signals. The area of the Lorentzian peak gives a measure of the intensity of the main transition cross section. The intensity of the multielectron transition resonance has been estimated from the area of the peaks which are left in the residual of Fig. 8. The area has been evaluated by fitting the residual peaks with a Lorentzian function convoluted with a Gaussian function accounting for the experimental resolution as determined previously. The experimental values of the ratio between the double- and the single-electron cross section are compared with the theoretical predictions in Table I. This is of course only a coarse estimate and is reported to give a qualitative idea of the agreement between the experimental results and the theoretical values. The experimental intensity ratios are lower than the calculated ones in agreement with the results obtained for some elements of the rare-earth series.[13,14]

The Ba-O and Ba-H peak parameters obtained from the fitting procedure are listed in Table II. After the minimiza-

TABLE II. Structural parameters of the Ba-O and Ba-H asymmetric peaks obtained from the EXAFS analysis: R represents the average distance, σ^2 represents the vibrational variance, β is the asymmetry parameter, and N is the coordination number. The standard deviations are given in parentheses.

	R (Å)	σ^2 (Å^2)	β	N
Ba-O	2.780 (0.003)	0.012 (0.008)	0.02 (0.14)	7.8 (0.3)
Ba-H	3.44 (0.02)	0.03 (0.01)	0.65 (0.15)	18 (7)

tion the structural parameters have been found to be slightly different from the MD starting values; in particular the $g_{\mathrm{Ba,O}}(r)$ and $g_{\mathrm{Ba,H}}(r)$ first peaks were found to be shifted to shorter distance and the Ba-O coordination number to be lower. X-ray-diffraction (XRD) and EXAFS investigations were previously carried out by Persson *et al.*[19] on a 0.82 M Ba^{2+} aqueous solution. From the XRD analysis a Ba-O shell distance of 2.82 Å and a coordination number of 8.1 have been obtained. The EXAFS data analysis was carried out without minimizing the coordination number due to the $\chi(k)$ amplitude distortion associated with the opening of the multielectron excitation channels. Note that the Ba-O shell distance obtained from the XRD investigation cannot be directly compared with the value in Table II. In the present EXAFS analysis the Ba-O first shell peak is modeled with an asymmetric peak where R is the average distance and not the modal value of the distribution.

The zero positions of the theoretical energy scales were found at 5254.1 ± 0.2, 5631.5 ± 0.3, and 6001 ± 1 eV for the L_3, L_2, and L_1 cross section, respectively. The S_0^2 values were found to be equal to one for the three edges.

Particular attention has to be paid to the accuracy of the structural parameters listed in Table II. A thorough description of a correct procedure for error evaluation is described in Ref. 41. By neglecting systematic errors in the experimental data and in the theory, the error affecting the fitted parameters can be estimated on the basis of statistical concepts. Standard deviations and correlated effects can be evaluated by using correlation maps for each couple of parameters. Contour maps showing the correlated errors associated with a 95% confidence interval are presented in Fig. 11, for some relevant parameters. A positive correlation has been found between the E_0 values and R_{O}, σ_{O}^2 and N_{O}, and R_{O} and β_{O}, while there is no correlation between the other possible parameter couples associated with the Ba-O shell. From the present analysis the errors affecting the Ba-H shell parameters have been found to be larger, due to the strong correlation between σ_{H}^2 and N_{H} and between R_{H} and β_{H}. This effect is responsible for the large uncertainty of the Ba-H coordination number. This is not surprising as the amplitude of the Ba-H contribution is small and the data range of the detectable signal is narrow.

The high sensitivity of the EXAFS technique to the low-distance range of the $g(r)$ first peak is shown by the low errors obtained for the Ba-O peak parameters. This allowed a very accurate determination of the short-range properties of the Ba-O $g(r)$. On the contrary, the refinement of the short-distance shape of the Ba-H MD $g(r)$ on the basis of the EXAFS information is hampered by the low accuracy of the refined structural parameters.

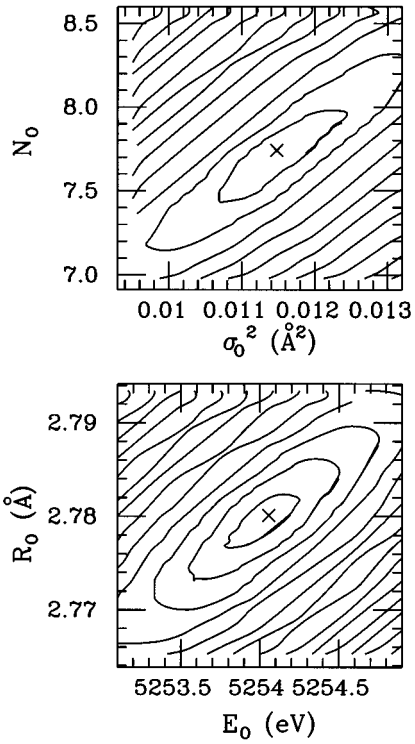

FIG. 11. E_0R_{O} (lower panel) and $\sigma_{\mathrm{O}}^2\,N_{\mathrm{O}}$ (upper panel) correlation maps showing the statistical errors on the Ba-O first-shell parameters. The inner elliptically shaped curves represent the 95% confidence interval.

A general remark should be made on the improvement of the EXAFS data analysis which is achieved by performing a multiedge refinement. To this end we have applied a fitting procedure to the three L edges, separately. In the case of the $L_{2,3}$ edges the fitted parameters obtained from the separate refinements are equal to those reported in Table II. An increase of about 20% has been found for the errors associated with distances and coordination numbers. As far as the L_1 edge is concerned, a satisfactory determination of the structural parameters is hampered by the larger signal-to-noise ratio of the spectrum. Therefore, the aid of the multiedge analysis was essential to perform a reliable characterization of the double-electron excitation resonance above the L_1 edge.

Finally, we discuss the implication of the double-electron features relative to the EXAFS data analysis. A fitting procedure has been applied to the EXAFS spectra extracted with a conventional three region polynomial spline function. The results are shown in Fig. 12. The agreement between experiment and theory is not satisfactory ($R=0.549\times10^7$) and the residual curves show the presence of anomalous structures at the energies of the $L_{2,3}N_{4,5}$ and $L_1N_{4,5}$ edges. The refined parameters obtained from the minimization are $R_{\mathrm{O}}=2.770$ Å, $\sigma_{\mathrm{O}}^2=0.012$ Å^2, $\beta_{\mathrm{O}}=0.01$, $N_{\mathrm{O}}=6.9$, and $R_{\mathrm{H}}=3.43$ Å, $\sigma_{\mathrm{H}}^2=0.03$ Å^2, $\beta_{\mathrm{H}}=0.65$, $N_{\mathrm{H}}=12$. By comparing these values with those in Table II it appears that the coordination numbers are underestimated and the shell distances are slightly lower when double-excitation effects are not included. The same result has been obtained for Sr^{2+} and rare-earth ions in water solution.[9,13,14]

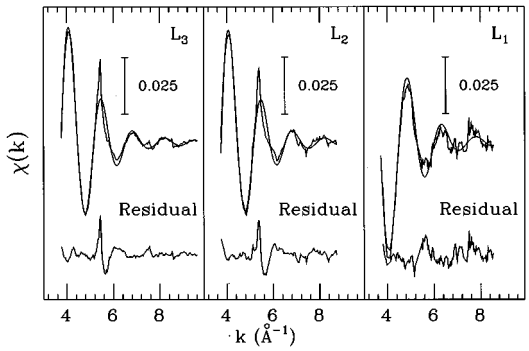

FIG. 12. Comparison of the total L-edge theoretical signals with the experimental $\chi(k)$ experimental spectra extracted without the inclusion of the double-excitation edges. The residual curves show the presence of features which are associated with the opening of the double-electron excitation channels.

VII. CONCLUSIONS

A detailed x-ray-absorption investigation of a Ba^{2+} aqueous solution above the L edges was carried out with the aim to characterize the double-electron excitation resonances appearing in the EXAFS spectra. The L_3, L_2, and L_1 edge EXAFS spectra have been analyzed simultaneously in the correct framework of the radial distribution theory. The Ba-O and Ba-H signals have been calculated starting from realistic $g(r)$ models obtained from MD simulations. The existence of double-excitation channels at the Ba L edges has been clearly shown. These resonances are attributed to the excitation of a secondary electron coming from a $4d$ level. The experimental values of the energy onset of the $2p4d \rightarrow (5d)^2$ transition, in the case of the L_3 and L_2 spectra, and of the $2s4d \rightarrow 6p5d$, in the case of the L_1 spectrum, are in good agreement with theoretical calculations. The combined L-edge analysis was essential for an unambiguous identification of the double-electron excitation affecting the L_1 edge. The multiedge analysis allowed reliable structural information to be obtained also if only a narrow energy region is available. The presence of multielectron excitations distorts the EXAFS data analysis leading to systematic errors on the structural parameters and in an underestimation of the coordination number. The results of the present investigation provide a guideline for the correct structural analysis of the EXFAS spectra above the L edges of rare-earth ions in aqueous solutions.

ACKNOWLEDGMENTS

The authors gratefully acknowledge Dr. Andrea Di Cicco for helpful suggestions on the use of the FITHEO program for the multiedge data analysis. We thank the European Union for support of the work at EMBL Hamburg through the HCMP Access to Large Installation Project, Contract No. CHGECT930040. Paola D'Angelo was supported by EU Contract No. ERBCHBGCT930485. This work was sponsored by the Italian Consiglio Nazionale delle Ricerche and by the Italian Ministero per l'Università e per la Ricerca Scientifica e Tecnologica.

[1] S. J. Schaphorst, A. F. Kodre, J. Ruscheinski, B. Crasemann, T. Åberg, J. Tulkki, M. H. Chen, Y. Azuma, and G. S. Brown, Phys. Rev. A **47**, 1953 (1993), and references therein.

[2] J. M. Esteva, B. Gauthé, P. Dhez, and C. R. Karnatak, J. Phys. B **16**, L263 (1983).

[3] M. Deutsch and P. Kizler, Phys. Rev. A **45**, 2122 (1992).

[4] R. D. Deslattes, R. E. LaVilla, P. L. Cowan, and A. Henins, Phys. Rev. A **27**, 923 (1983).

[5] E. Bernieri and E. Burattini, Phys. Rev. A **35**, 3322 (1987).

[6] A. Filipponi, E. Bernieri, and S. Mobilio, Phys. Rev. B **38**, 3298 (1988).

[7] A. Filipponi, T. A. Tyson, K. O. Hodgson, and S. Mobilio, Phys. Rev. A **48**, 1328 (1993).

[8] P. D'Angelo, A. Di Cicco, A. Filipponi, and N. V. Pavel, Phys. Rev. A **47**, 2055 (1993); E. Burattini, P. D'Angelo, A. Di Cicco, A. Filipponi, and N. V. Pavel, J. Phys. Chem. **97**, 5486 (1993).

[9] P. D'Angelo, H.-F. Nolting, and N. V. Pavel, Phys. Rev. A **53**, 798 (1996).

[10] E. Giglio, S. Loreti, and N. V. Pavel, J. Phys. Chem. **92**, 2858 (1988).

[11] P. D'Angelo, A. Di Nola, E. Giglio, M. Mangoni, and N. V. Pavel, J. Phys. Chem. **99**, 5471 (1995).

[12] J. Chaboy, J. García, A. Marcelli, and M. F. Ruíz-Lopez, Chem. Phys. Lett. **174**, 389 (1990).

[13] J. A. Solera, J. García, and M. G. Proietti, Phys. Rev. B **51**, 2678 (1995).

[14] J. Chaboy, A. Marcelli, and T. A. Tyson, Phys. Rev. B **49**, 11 652 (1994).

[15] J. Chaboy and T. A. Tyson, Phys. Rev. B **49**, 5869 (1994); J. Chaboy, T. A. Tyson, and A. Marcelli, *Relative Cross Sections for Bound-State Double-Electron $LN_{4,5}$-Edge Transitions of Rare Earths and Nonradioactive Elements of the Sixth Row*, (Prensas Universitarias de Zaragoza, Zaragoza, 1995), p. 149.

[16] A. Kodre, I. Arcon, M. Hribar, M. Stuhec, F. Villain, W. Drube, and L. Tröger, Physica B **208&209**, 379 (1995).

[17] G. G. Li, F. Bridges, and G. S. Brown, Phys. Rev. Lett. **68**, 1609 (1992); A. I. Frenkel, E. A. Stern, M. Qian, and M. Newville, Phys. Rev. B **48**, 12 449 (1993).

[18] P. D'Angelo, A. Di Nola, A. Filipponi, N. V. Pavel, and D. Roccatano, J. Chem. Phys. **100**, 985 (1994).

[19] I. Persson, M. Sandström, H. Yokoyama, and M. Chaudhry, Z. Naturforsch. **50a**, 21 (1995).

[20] A. Di Cicco, Phys. Rev. B **53**, 6174 (1996).

[21] H. J. C. Berendsen, J. P. M. Postma, W. F. van Gunsteren, A. Di Nola, and J. R. Haak, J. Chem. Phys. **81**, 3684 (1984).

[22] W. F. van Gunsteren and H. J. C. Berendsen, Groningen Molecular Simulation (GROMOS) Library Manual, Biomos, Groningen, 1987.

[23] J. Åqvist, J. Phys. Chem. **94**, 8021 (1990).

[24] H. J. C. Berendsen, J. P. M. Postma, W. F. van Gunsteren, and J. Hermans, in *Intermolecular Forces*, edited by B. Pullmann (Reidel, Dordrecht, 1981), p. 331.

[25] J. G. Ryckaert, G. Ciccotti, and H. J. C. Berendsen, J. Comput. Phys. **23**, 327 (1977).

[26] E. Spohr, G. Pálinkás, K. Heinzinger, P. Bopp, and M. M. Probst,

J. Phys. Chem. **92**, 6754 (1988).
[27] W. Dietz, W. O. Riede, and K. Heinzinger, Z. Naturforsh. A **37**, 1038 (1982).
[28] G. Pálinkás, T. Radnai, W. Dietz, Gy. I. Szász, K. Heinzinger, Z. Naturforsh. A **37**, 1049 (1982).
[29] M. M. Probst, T. Radnai, K. Heinzinger, P. Bopp, and B. M. Rode, J. Phys. Chem. **89**, 753 (1985).
[30] Th. Kowall, F. Foglia, L. Helm, and A. E. Merbach, J. Phys. Chem. **99**, 13 078 (1995).
[31] C. Hermes, E. Gilberg, and M. H. J. Koch, Nucl. Instrum. Methods **222**, 207 (1984).
[32] R. F. Pettifer and C. Hermes, J. Phys. Paris Colloq. **47**, C8-127 (1986).
[33] R. F. Pettifer and C. Hermes, J. Appl. Cryst. **18**, 404 (1985).
[34] P. Eisenberger and G. S. Brown, Solid State Commun. **29**, 481 (1979).
[35] E. D. Crozier and A. J. Seary, Can. J. Phys. **58**, 1388 (1980).
[36] E. D. Crozier, J. J. Rehr, and R. Ingalls, in *X-ray Absorption: Principles, Applications, Techniques of EXAFS, SEXAFS and XANES*, edited by D. C. Koningsberger and R. Prins (Wiley, New York, 1988), Chap. 9.
[37] P. D'Angelo, A. Di Nola, M. Mangoni, and N. V. Pavel, J. Chem. Phys. **104**, 1779 (1996).
[38] A. Filipponi, A. Di Cicco, T. A. Tyson, and C. R. Natoli, Solid State Commun. **78**, 265 (1991); A. Filipponi, A. Di Cicco, and C. R. Natoli, Phys. Rev. B **52**, 15 122 (1995); A. Filipponi and A. Di Cicco, *ibid*. **52**, 15 135 (1995).
[39] L. Hedin and B. I. Lundqvist, J. Phys. C **4**, 2064 (1971).
[40] M. O. Krause and J. H. Oliver, J. Phys. Chem. Ref. Data **8**, 329 (1979).
[41] A. Filipponi, J. Phys. Condens. Matter **7**, 9343 (1995).